doi:10.1111/evo.14600

A common mechanism drives the alignment between the micro- and macroevolution of primate molars

Carrie S. Mongle,[1,2,3,4] Allison Nesbitt,[5] Fabio A. Machado,[6] Jeroen B. Smaers,[1] Alan H. Turner,[7] Frederick E. Grine,[1,7] and Josef C. Uyeda[6]

[1]*Department of Anthropology, Stony Brook University, Stony Brook, New York 11794*

[2]*Division of Anthropology, American Museum of Natural History, New York, New York 10024*

[3]*Turkana Basin Institute, Stony Brook University, Stony Brook, New York 11794*

[4]*E-mail: carrie.mongle@stonybrook.edu*

[5]*Department of Pathology and Anatomical Sciences, University of Missouri, Columbia, Missouri 65212*

[6]*Department of Biological Sciences, Virginia Polytechnic Institute and State University, Blacksburg, Virginia 24061*

[7]*Department of Anatomical Sciences, Stony Brook University, Stony Brook, New York 11794*

Received March 29, 2022
Accepted August 1, 2022

A central challenge for biology is to reveal how different levels of biological variation interact and shape diversity. However, recent experimental studies have indicated that prevailing models of evolution cannot readily explain the link between micro- and macroevolution at deep timescales. Here, we suggest that this paradox could be the result of a common mechanism driving a correlated pattern of evolution. We examine the proportionality between genetic variance and patterns of trait evolution in a system whose developmental processes are well understood to gain insight into how such alignment between morphological divergence and genetic variation might be maintained over macroevolutionary time. Primate molars present a model system by which to link developmental processes to evolutionary dynamics because of the biased pattern of variation that results from the developmental architecture regulating their formation. We consider how this biased variation is expressed at the population level, and how it manifests through evolution across primates. There is a strong correspondence between the macroevolutionary rates of primate molar divergence and their genetic variation. This suggests a model of evolution in which selection is closely aligned with the direction of genetic variance, phenotypic variance, and the underlying developmental architecture of anatomical traits.

KEY WORDS: Adaptive landscape, development, macroevolution, variation.

One of the primary factors considered to enable evolution at the microevolutionary scale is the existing genetic variance within a population. In particular, if one imagines a scenario in which genetic drift alone is operating on a population, genetic variance (G) is predicted to have a direct and proportional impact on evolutionary change, where a larger G would permit proportionally higher rates of phenotypic trait change in the population. Accordingly, several studies have demonstrated that the evolutionary divergence of traits between species occurs most rapidly in the direction of the highest genetic variance of a given trait within a species (Schluter 1996; Hunt 2007; Claverie and Patek 2013).

In this way, the relative genetic variance of a trait can be useful for predicting the kind of evolutionary change that it may undergo. Over short timescales, this is demonstrably true (e.g., Arnold and Phillips 1999; Blows and Higgie 2003). However, the proportionality between genetic variance and rates of evolutionary divergence is theoretically predicted to break down in response to directional selection ($\Delta\theta_M$) over longer timescales.

Paradoxically, recent experimental studies have demonstrated that the relationship between genetic variance and trait change can persist millions of years longer than the current theoretical framework would seem to suggest (Houle et al. 2017;

McGlothlin et al. 2018). One explanation for this persistence could be that the traits in question were not under natural selection (i.e., evolving only by genetic drift). However, this proposed explanation does not appear to be biologically realistic for functionally significant traits over timescales that range over millions of years (Lynch 1990).

This indicates that prevailing models of evolution cannot readily explain the link between micro- and macroevolution (Houle et al. 2017). Therefore, the apparent correlation between genetic variation and rates of trait evolution over deep time may not be the direct result of genetic constraint, but rather is most likely the result of a common mechanism that drives both the distribution of variation and the pattern of evolution. One possibility is that the adaptive landscape shapes the apparent correspondence between divergence and genetic variation by acting on the underlying developmental architecture of the traits in question (Alba et al. 2021). Indeed, recent studies suggest that epistatic interactions can potentially mold the structure of variation from mutation (and therefore the resulting **G**-matrix) to align with the adaptive landscape (Jones et al. 2014; Melo et al. 2016). However, these statistical models are largely detached from our knowledge of the underlying developmental architecture of the traits in question. Here, we evaluate how proportionality between divergence and genetic variation might be maintained over macroevolutionary time in a biological system whose developmental processes are known to structure variation. Specifically, we estimate rates of evolution along the molar developmental axis, and then test matrix proportionality between an evolutionary rate matrix ($\mathbf{\Sigma}$) with approximations of the additive genetic variance/covariance matrix (**G**) for dental traits.

Role of Development

Development serves as the link between the genotype and the phenotype by channeling the variation that is exposed to natural selection (Wagner 1988). Frequently, this variation is nonrandom. For example, in developmental processes that proceed segmentally along an axis, such as limbs and vertebrae, it has been demonstrated that an element's position in the developmental sequence can impact its phenotypic (and inferred genetic) variation (Young et al. 2015). Traits with more genetic variation are expected to evolve at a faster rate (i.e., be more "evolvable") than those with less variation (Wagner 1988), which suggests that developmentally biased variation could impact rates of evolution at a macroevolutionary scale.

Although much is known about the principles that govern each of the individual levels of biological variation (i.e., developmental, population genetics, macroevolution), most studies address only one or two of these levels. A central challenge for biology is to reveal how these different levels of variation interact and jointly shape diversity (Jernvall and Jung 2000). Here, we consider how the biased variation generated by developmental processes is expressed at the population level, and how population-level variation and genetic variance manifest through evolution across species.

Mammalian molar teeth present a model system for linking developmental processes to evolutionary dynamics because of the biased pattern of variation that results from the regulation of their formation (Polly and Mock 2017). Like other serially patterned anatomical structures, molars develop sequentially (mesially to distally). The development of mammalian teeth is initiated when the dental lamina begins to form as a thickened strip of epithelium above the underlying mesenchymal tissue (Jernvall and Thesleff 2000). Within the molar region, the epithelial signaling center (i.e., the primary enamel knot) of the first molar (M1) is the first to develop within the dental lamina (Jernvall and Thesleff 2000). The primary enamel knot of the M2 then begins to form in the tail of the dental lamina posterior to the M1, a process that sequentially repeats until the last molar is initiated (Jernvall and Thesleff 2000).

Kavanagh et al. (2007) have demonstrated experimentally that the sequential initiation of each molar is dependent on the previous molar through a reiterative process of intermolar inhibition and mesenchymal activation. According to this model, the surrounding mesenchymal tissue produces activation factors for molar growth, whereas the primary enamel knot produces inhibitory factors that limit the growth of subsequent teeth (Kavanagh et al. 2007). This cascading relationship of signaling molecules has been deemed the "Inhibitory Cascade" (IC).

A key prediction of the IC model is that molar size proportions are determined by the relative strengths of activating and inhibitory interactions, such that weak levels of inhibition with high levels of activation produce a pattern of M1 < M2 < M3, whereas high levels of inhibition paired with low levels of activation produce a pattern of M1 > M2 > M3 (Kavanagh et al. 2007). Others have found that the relative strengths of activating and inhibitory interactions also predict relative molar complexity, with lower levels of inhibition resulting in a linear increase in complexity moving distally along the tooth row (Selig et al. 2021). In addition to patterning size proportions and complexity along the molar row, this developmental pattern of repeated activation is predicted to produce cumulative variation in later developing segments (Jernvall and Jung 2000; Selig et al. 2021).

The resulting pattern of dental variation, whereby earlier developing molars are less variable than those that develop later, has long been observed at the species level across a wide range of mammals (e.g., Butler 1939; Hlusko et al. 2011; Gómez-Robles and Polly 2012). This pattern is exemplified by the modern human dentition, which shows almost no variability in the presence

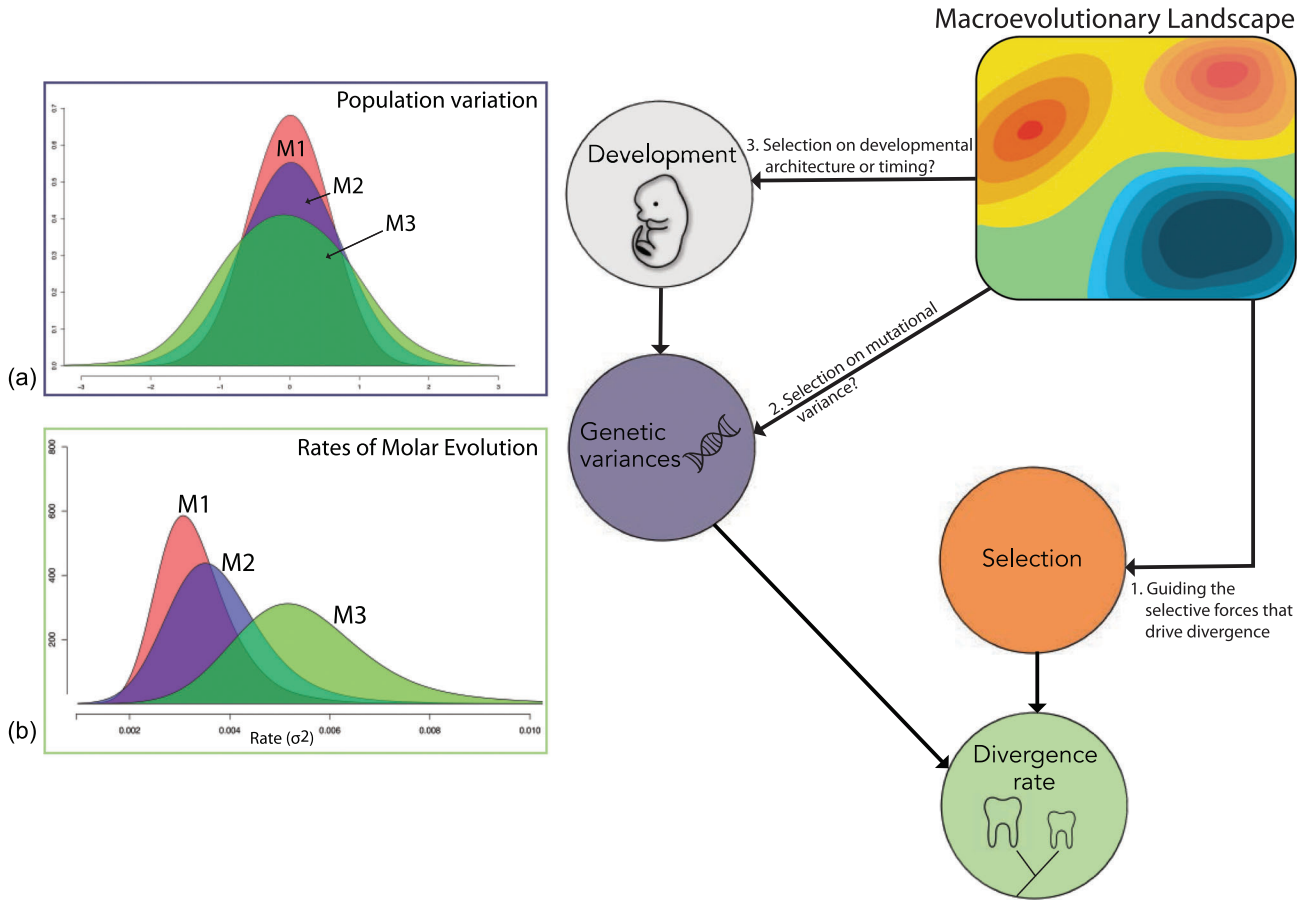

Figure 1. **Distributions in panel (a) depict population-level phenotypic variation in the M1–M3. Distributions were linearly transformed to center on 0 to demonstrate overlap of variance along the *x*-axis. The distributions in panel (b) are the posterior distributions of the rates (σ^2) of primate molar evolution (M1–M3, MD dimension). These rates were estimated for each molar using a reversible-jump Brownian motion model. For the rates of M1–M3 evolutionary divergence to be directly proportional to the phenotypic and genetic variances, this suggests a common mechanism in which the macroevolutionary landscape simultaneously shapes the selective forces driving rates of divergence (arrow 1) and mutational variation (arrow 2); possibly via direct selection on the developmental architecture of the inhibitory cascade (arrow 3).**

of the first molar but considerable variability in the presence or absence of the third (the "wisdom tooth").

Importantly, however, evolution happens at the population level. So, although it is significant that this pattern of dental variation has been observed broadly across different mammalian species, it is essential that it also be observable within a population for it to have relevance for evolution by natural selection (Hlusko 2004; Hlusko et al. 2016).

Materials and Methods

SEQUENTIAL ACCUMULATION OF GENETIC VARIANCE

To establish population-level variation, phenotypic variances (V_p) were extracted from a recent study that investigated dental genetic architecture in a breeding population of hamadryas baboons (Hlusko et al. 2011). This provides a window to examine whether dental variance in a population increases along the axis of development. These data demonstrate that, despite the high genetic covariance among molars, phenotypic variance of both mesiodistal length (MD) and buccolingual breadth (BL) is lowest in the M1 (BL $V_p = 0.28$; MD $V_p = 0.33$), intermediate in the M2 (BL $V_p = 0.49$; MD $V_p = 0.66$), and highest in the M3 (BL $V_p = 0.63$; MD $V_p = 1.58$) (reported variances calculated from measurements [mm] of left side molars; Fig. 1a).

Building on these developmental and population-level insights, we tested whether the IC structures the evolvability of molar teeth on a macroevolutionary scale. This analysis spans the clade of anthropoid primates (Old World monkeys, New World monkeys, apes) which encompasses approximately 52 million years of evolution (Steiper and Seiffert 2012). The phylogenetic relationships of these taxa are represented by a Bayesian posterior distribution of trees constructed from aligned molecular sequence data (Arnold et al. 2010; Fig. S1).

Trait data in this study consist of standard MD and BL measurements of primate mandibular molar crowns. These were taken from a large dataset ($N > 3200$ individuals) of physical measurements provided by Plavcan (1990), who preferentially recorded measurements from the right side. These data were log-transformed and then summarized into species means that were used in subsequent analyses. After matching the phylogeny to the trait data, the final dataset consisted of 105 anthropoid primate species. These mean values, along with their standard errors, are provided in Table S1.

We calculated the phylogenetic signal of the traits using the multivariate extension of the Bloomberg's *K* statistic (*K*-mult; Adams 2014). Because *K*-mult assumes a Brownian motion (BM) model of evolution, it can be used to infer the adequacy of BM to model phenotypic evolution (see below). Low values of *K*-mult imply a lack of phylogenetic signal under BM, whereas values closer to 1 are expected under a BM model of evolution. To account for phylogenetic and sampling uncertainty, we performed a parametric bootstrap procedure by drawing species means and standard errors 1000 times. Each draw was then paired to a sample of the posterior distribution of trees, resulting in a distribution of *K*-mult values. For this analysis, we excluded species with missing M3s.

We log-transformed the phenotypic and genetic variances from Hlusko et al. (2011) with the formula $\sigma^2_{\ln} = \ln(\sigma^2/\bar{z}^2 + 1)$, where σ^2 is the raw scale variance and $\bar{z}$ is the raw scale mean. The BL and MD measurements were analyzed independently for each tooth in a set of univariate analyses, and then in a multivariate framework together with estimates of the additive genetic variance of each trait. Using this two-pronged approach, we were able to first simplify parameter space and consider just the sequential accumulation of genetic variance and evolutionary divergence across the three molars, and then subsequently examine the role of trait interaction and potential sources of uncertainty (e.g., measurement error, phylogenetic uncertainty, and estimates of trait covariance and heritability [h^2]) in a more complex set of models.

MACROEVOLUTIONARY RATES OF MOLAR EVOLUTION (UNIVARIATE)

In the univariate analyses, trait evolution was modeled as a random-walk BM process (Felsenstein 1973), and rate was estimated as the magnitude of undirected, stochastic variance (σ^2). As such, traits with more developmental variation are expected to evolve at a faster rate, but there is no a priori prediction about the specific trajectory of evolution that will be followed. Rather, a greater value in this parameter (σ^2) simply equates to a greater accumulation of trait change over time (e.g., greater phylogenetic variation). We employed three different univariate approaches to model this process:

Constant-variance Brownian motion

This represents the standard BM model, which assumes that average trait change is proportional to the square root of time and that the rate of evolution is stochastically constant such that it has a single mean and variance across all branches on the phylogeny. This procedure, implemented in the R package "phytools," uses a Bayesian Markov chain Monte Carlo (MCMC) to sample from the posterior distribution for the states at internal nodes in a tree that is based on available phenotypic and phylogenetic information at the terminal tips (Revell 2012). This analysis was conducted separately for each individual molar measurement (BL and MD of M1–M3). In each molar analysis, the MCMC was run for 10 million generations, with 20% burn-in discarded. Rate was estimated as the mean from the posterior distribution of tree-wide σ^2 values.

Reversible-jump Brownian motion

This implementation of a BM model allows for variable rates of evolution by using a reversible-jump MCMC procedure to estimate the number of different rates across a tree (Pagel and Meade 2007). In this analysis, implemented in the software "BayesTraits," the MCMC chain was run for 10 million generations with 20% discarded as burn-in. This analysis was conducted separately for each individual molar measurement (M1–M3 MD and BL). Chain convergence was assessed in Tracer version 1.6.0 (Rambaut et al. 2014). Following the reversible-jump Brownian motion analysis, a tree-wide evolutionary rate (σ^2) was estimated for each molar from the average branch-specific sigma-squared values.

Permutation test

Finally, rates of evolution were directly compared between molars (M1 vs. M2, M2 vs. M3, and M1 vs. M3) using a permutation test. This method, which was also conducted within a BM framework, calculates the rate of evolution from the sum of the squared Euclidean distances between the phylogenetically transformed trait values at the tips of the tree and the estimated ancestral state at the root of the tree. To compare rates of evolution among different traits, we followed the procedure outlined by Denton and Adams (2015) in which statistical differences are estimated by simulating data across the tree under the null hypothesis of a single rate. These were then compared using observed and simulated rate ratios between traits. This procedure was implemented in the R package "geomorph."

PROPORTIONALITY OF GENETIC VARIANCE (MULTIVARIATE)

To test for genetic constraint in the trajectory of anthropoid molar evolution, we compared the evolutionary rate matrix ($\mathbf{\Sigma}$) with approximations of the additive genetic variance/covariance

matrix (**G**) for dental traits recorded by Hlusko et al. (2011). **Σ** is a square matrix, which summarizes the rates of evolution (diagonals) of each trait and the covariance of rates among traits (off-diagonals) under a multivariate BM model (Felsenstein 1988). **G** is also a square matrix that summarizes the amount of additive genetic variance of each trait (diagonals) and covariance (off-diagonals) among traits. A close correspondence between **Σ** and **G** would be expected if the patterns of genetic variation among traits constrain the macroevolutionary patterns of diversification (Felsenstein 1988, 2008; Houle et al. 2017).

For anthropoid teeth, correlations among traits estimated from phenotypic distributions have been shown to be good approximations of genetic correlations (Hlusko and Mahaney 2009; Hardin 2019, 2020), a phenomenon that has been referred to as the "Cheverud Conjecture" (Cheverud 1988; Roff 1995). Although genetic constraint models (see Houle et al. 2017) make predictions based on either **G** or the mutational variance-covariance matrix **M** (which is unavailable), it is less clear whether, in practice, **G** or **P** will be more predictive of macroevolutionary divergence. This is because genetic variation may vary over time, and a single point estimate of **G** from one species may be less representative of long-term average values than pooled **P** matrices. In addition, although nonheritable environmental variances are not expected to affect genetic drift or response to selection, functional adaptive landscapes could favor developmental architectures that channel environmental variation into regions of morphospace that maintain functional integration. This could also result in **P** being more predictive of evolution on those landscapes than **G**. In practice, disentangling these possibilities is challenging (e.g., distinguishing estimation error from evolutionary stochasticity). Therefore, we use multiple approaches to test for the correspondence within-species covariance and divergence. We employed estimates of the phenotypic variance/covariance matrix (**P**) as an initial approximation of the full multivariate **G**, combined with direct estimates of trait heritability from Hlusko et al. (2011). It should be noted that this approach assumes that **P** is shared across the species included in our sample or, alternatively, that the pooled average estimates the long-term value over macroevolutionary time. Details of the procedure to estimate **P** and the approximation of **G** are provided in the Supporting Information.

To compare estimates of **G** and **P** to the BM evolutionary rate matrix Σ, we modeled Σ as being either proportional to a target matrix (henceforth "proportional model"), or fully estimated (henceforth "full model") through maximum likelihood (Hohenlohe and Arnold 2008; Revell and Harmon 2008). We fitted proportionality and full models under two conditions. First, we estimated the diagonal elements of Σ (henceforth "diagonal models") and second, we modeled a full Σ with the diagonal and off-diagonal elements (henceforth "covariance models"). Although the first focus on the central prediction of the IC (i.e., that variance increases along the molar row), the second evaluates the possible effects of covariances on trait evolution. Models were fit using the PCMFit package (Mitov et al. 2019; Mitov et al. 2020), which uses species average phenotypes, measurement errors, and a phylogenetic hypothesis to calculate optimal model parameters under a maximum likelihood framework. Because the proportionality models were not implemented in the basic PCMFit pipeline, we developed an add-on package that incorporates this model (PCMkappa; https://github.com/FabioLugar/PCMkappa).

To account for phylogenetic uncertainty, we performed the analysis on 1000 samples from the posterior distribution of phylogenies provided by Arnold et al. (2010). For the proportional models, each posterior sample of the **P** and **G** was randomly paired with one sample from the tree distribution, resulting in 1000 tree-**P/G** combinations that incorporate phylogenetic, variance, and h^2 uncertainties. We obtained likelihoods for each of the 6000 resulting fits (1000 full model, 1000 proportional to **P**, and 1000 proportional to **G**, as well as 1000 for each of the covariance and diagonal models). Model comparisons were performed using the Bayesian information criterion (BIC) as the Akaike information criterion (AIC) can spuriously favor more complex models as the amount of data increase (Dennis et al. 2019). The resulting distribution of Σ was compared to the distribution of Gs and Ps using Principal component similarity (Melo et al. 2015), which compares covariance matrices according to the alignment of their principal components and similarity in the distribution of variance along those components. Values close to 0 indicate that the matrices do not share any structural similarity, whereas values close to 1 mean that matrices are similar in both the direction and in the distribution of variation. Similarity of variance distribution means that matrices' eigenvalues are roughly in the same order, but not necessarily proportional. In other words, two matrices can have a value of 1 if they share the same eigenvectors and their eigenvalues are sorted in the same order.

To evaluate if the proposed tests have sufficient power to reject the proportionality between **G/P** and Σ, we examined the likelihood surface in the case of the diagonal model using only MD or BL dimensions separately (Supporting Information). This was done to simplify power simulations over the parameter space, and because the diagonal models were the only ones that failed to reject proportionality (see *Results*).

Finally, because the IC predictions are based on the overall area of molars, rather than linear measurements, we approximated the rates of evolution and variances (phenotypic and genetic) for the areas of each molar. On the logarithmic scale, the area variance can be approximated as $\sigma^2_a = \sigma^2_{BL} + \sigma^2_{MD} + 2\sigma_{BLMD}$, where σ^2_{BL} and σ^2_{MD} are the variance for BL and MD, respectively, and σ_{BLMD} is the covariance between BL and MD.

Because this requires the covariance between linear measurements, this calculation was only done for Σ estimated on the full covariance model and on the pooled within-group **P** obtained from the Plavcan (1990) dataset and the **G** approximated from **P**.

Results

RATES OF EVOLUTION INCREASE ALONG A DEVELOPMENTAL AXIS

The dental metrics used in this study display high phylogenetic signal, with the 95% interval of the bootstrapped values falling between 1.080 and 1.414. This justifies the use of BM as the model of evolution. Concordant with predictions, the evolutionary rate analyses demonstrate that variance increases along the molar row (Table 1). Results show that the earliest developing molar (M1) evolves at the slowest rate across taxa, the second molar (M2) was found to evolve at a slightly faster rate than the M1, and the last developing molar (M3) was found to evolve at the fastest rate. These results hold independent of the method used, for both univariate and multivariate approaches (Table 1). The distribution of variance is consistent with the levels of genetic variance estimated from Hlusko et al. (2011), which also increases sequentially along each molar M1–M3, even on the logarithmic scale (Table 1; Fig. 2).

RATES OF EVOLUTION ARE PROPORTIONAL TO GENETIC AND PHENOTYPIC VARIANCE

In the analysis where only the diagonal entries of the matrix were evaluated, BIC comparisons failed to differentiate between the full model and the proportional models in which rates were constrained to be proportional to either the genotypic or phenotypic variances (Fig. 2). Indeed, estimates of the evolutionary rates on the full diagonal model are remarkably close to the within-population variances (Table 1). However, when we evaluated the multivariate models that include trait covariances, the full model outperforms the proportionality models, even after accounting for parameter inflation through BIC (Fig. 3). Despite this, the comparison between the evolutionary rate matrices for the full covariance model and Ps and Gs showed high similarity values (Fig. 4). This implies that the main directions of variance distribution are shared between matrix types. Furthermore, the evolutionary rates (diagonal entries) for the full covariance model are very similar to within patterns of variation, for individual molar dimensions (Table 1; Fig. 1) as well as for molar areas (Fig. 2), suggesting that the differences lie in the magnitude of association between traits (covariances) (see Supporting Information).

In the simplified version of the models that examined only the proportionality of individual MD or BL dimensions, the

Table 1. **(A) Results of univariate and multivariate evolutionary rate analyses for each molar estimated from the Plavcan (1990) dataset, compared with (B) direct estimates of genetic and phenotypic variance in log-scale of baboon molar measurements taken from Hlusko et al. (2011). Values in parenthesis are standard deviations obtained for distributions of parameters.**

	M1 BL σ^2	M2 BL σ^2	M3 BL σ^2	M1 MD σ^2	M2 MD σ^2	M3 MD σ^2
(A) Macroevolutionary Rates:						
Constant-variance Brownian motion	0.0027	0.0029	0.0038	0.0029	0.0032	0.0049
Reversible-jump Brownian motion	0.0029	0.0033	0.0046	0.0034	0.0037	0.0055
Permutation	0.0024	0.0028	0.0037	0.0028	0.0031	0.0046
Full multivariate diagonal model	0.00268 (0.00009)	0.00334 (0.00011)	0.00447 (0.00015)	0.00279 (0.00012)	0.00330 (0.00017)	0.00360 (0.00020)
Full multivariate covariance model	0.00277 (0.00069)	0.00343 (0.00087)	0.00509 (0.00125)	0.00281 (0.00070)	0.00342 (0.00089)	0.00444 (0.00115)
(B) Within-Population Variances:						
Genetic variances	0.00218	0.00206	0.00212	0.00172	0.00169	0.00213
Residual phenotypic variances	0.00402	0.00382	0.00418	0.00195	0.00224	0.00395
Phenotypic variances	0.00481	0.00567	0.00659	0.00287	0.00420	0.00682

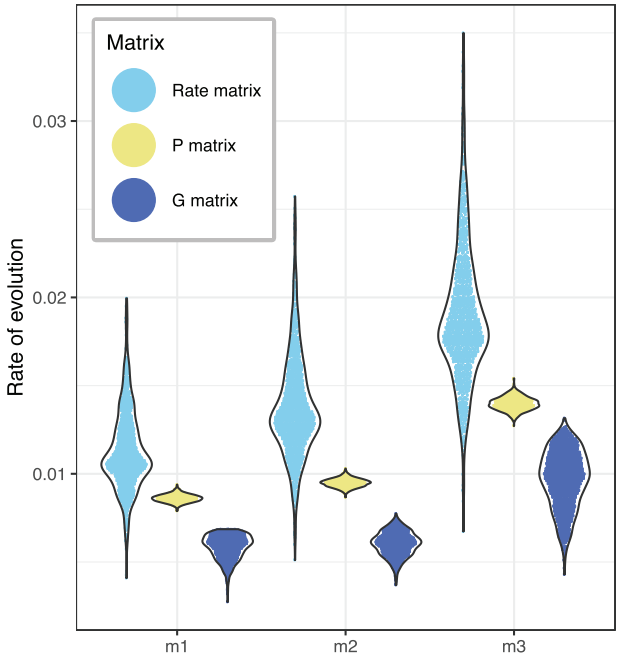

Figure 2. **Violin plots depicting the posterior distributions of rate estimates (σ^2) from each of the multivariate Brownian motion models that were fit to the log-molar areas. The rate estimates from the full model (BM) are shown in light blue, whereas estimates from the model proportional to the P-matrix ($\Sigma \sim P$) are in yellow, and rate estimates from the model proportional to our estimate of multivariate G ($\Sigma \sim G$) are in dark blue.**

estimates obtained from the divergence data were nearly identical to those directly estimated from a model where rates are proportional to phenotypic variances (Table S2). When these estimates are plotted on the likelihood surface for the macroevolutionary data (Fig. S2), the likelihood surface specifies a relatively small area of fit from the comparative data for which proportionality fails to be rejected. Estimates of genetic and phenotypic variances are both found within this area, even after accounting for errors in estimation.

Discussion

The results of this study suggest that there is a strong correspondence between macroevolutionary rates of evolution and phenotypic variation at the population level. This holds irrespective of the type of analysis (univariate or multivariate), the complexity of the model (diagonal or covariance classes of models), or the incorporation of within-species parameter estimation and phylogenetic errors (Table 1). Model selection approaches show that rates of evolution are directly proportional to both genetic and phenotypic variance (Fig. 3). The incorporation of information about trait covariance breaks the direct proportionality between within-species variation and macroevolutionary rates (Fig. 3), but does not significantly alter the correspondence between trait variance and evolutionary rates (Table 1; Fig. 2). Furthermore, rate matrices (Σ) and within-population patterns of variation (**G** and **P**) share high structural similarities (eigenvector and eigenvalue structures; Fig. 4), suggesting that evolution occurs principally along the lines of genotypic and phenotypic variation (Schluter 1996).

The present findings provide a link between different scales of biological variation and suggest that developmental processes may play a role in maintaining proportionality between genetic variation and evolutionary divergence over macroevolutionary time. Specifically, our results could be interpreted as demonstrating that the evolvability of anthropoid molar teeth has been biased by the inhibitory cascade, whereas the trajectory of evolution has occurred in the direction of genetic variance. However, it is surprising that these simple genetic constraints could bias functional traits under selection over millions of years. Quantitative genetic studies in mice have demonstrated the existence of segregating variation in quantitative trait loci that can alter the relationship among molars away from what is predicted by the inhibitory cascade model (Navarro and Maga 2018). This suggests that genetic variation can overcome such constraints. Furthermore, bias in the production of variation imposed by genetic and ontogenetic associations among traits is expected to be relatively short lived (Schluter 1996), raising the question of how these constraints are expressed over longer timescales. This kind of direct proportionality between rates of divergence and genetic variance is expected to exist transiently during an adaptive walk, or under pure genetic drift, but is not expected to affect the diversification of functionally important molars under constant selection. Our results suggest that the close concordance of evolutionary divergence with genetic variance is driven by a common mechanism, in which the macroevolutionary landscape simultaneously shapes the selective forces that drive rates of divergence (Fig. 1, arrow 1) and mutational variation (Fig. 1, arrow 2). This mechanism is possibly via direct selection on the developmental architecture of the inhibitory cascade (Fig. 1, arrow 3).

Such a mechanism is consistent with the theory that phenotypic diversity over macroevolutionary timescales is shaped by selection to conform to the adaptive landscape (McGlothlin et al. 2018). Interestingly, phenotypic variances show stronger proportionality than genetic variances to macroevolutionary rates (Tables 1 and S2). This could be because phenotypic variances are estimated with less uncertainty, or it could reflect a real biological signal where phenotypic variances are more predictive of macroevolutionary rates. Indeed, on the log scale, genetic variances for successive molars (Hlusko et al. 2011) do not appear to increase as substantially from M1–M3 as phenotypic variances (or macroevolutionary rates). Instead, the increase in phenotypic variance appears to be driven primarily by increased

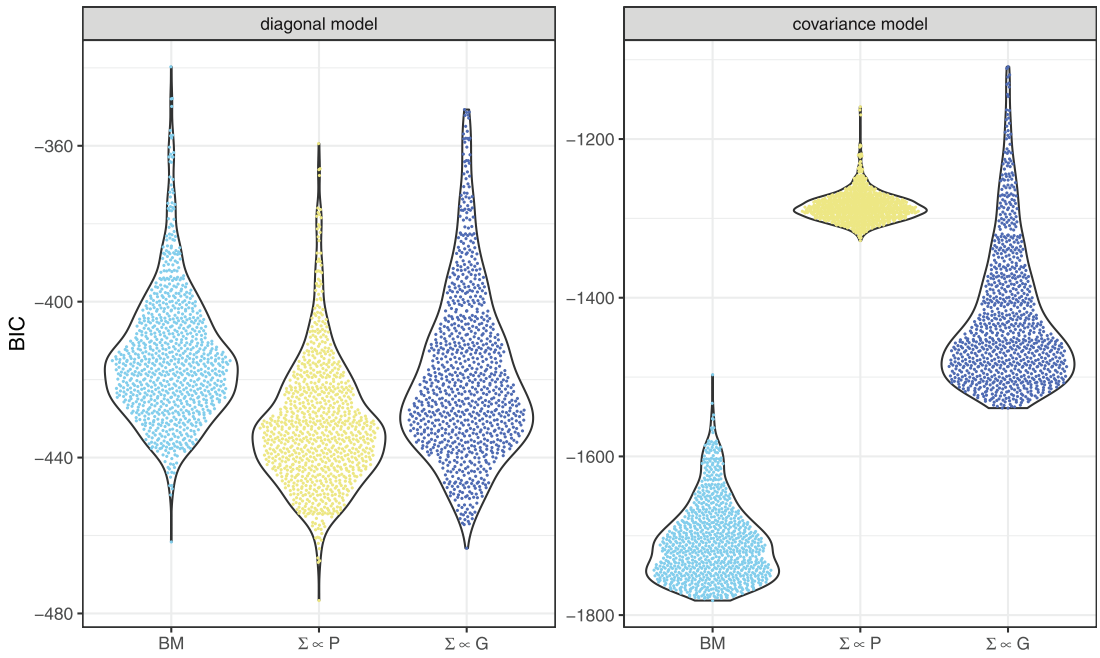

Figure 3. Violin plots showing comparisons of multivariate Brownian motion models fit to log-molar areas using the full model (BM) and two proportional models, one proportional to the P-matrix ($\Sigma \sim P$) and the other proportional to our estimate of multivariate G ($\Sigma \sim G$). Models were evaluated for a reduced diagonal model, including only variances, and a covariance model, accounting for the full covariance matrices. Violin plots show distribution of BIC values after accounting for phylogenetic and matrix uncertainty.

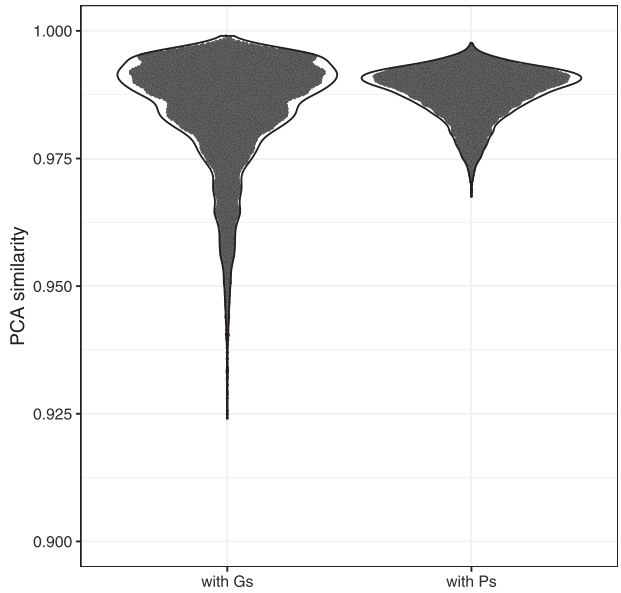

Figure 4. Principal component similarity values between a sample of the distribution of rate matrices and samples of P and G matrices. For simplicity, we only show the pairwise values for 100 randomly selected pair of matrices for each comparison.

environmental (i.e., nongenetic) variation for each successive tooth. This makes sense from a developmental perspective, particularly in species with extended periods of time between the formation and eruption of successive molars. It also suggests that the developmental pathway of the inhibitory cascade reinforces sequential increases in genetic, environmental, and phenotypic variation.

Although previous empirical and simulation studies have demonstrated a concordance between genetic variation and macroevolutionary divergence (Jones et al. 2014; Houle et al. 2017; McGlothlin et al. 2018), these studies have lacked a mechanistic appreciation of the process of development itself, which is also under selection. By studying anthropoid molars and the well-understood inhibitory cascade, we can better understand what drives the concordance of variation across scales. It has been suggested that early stages of development are subject to higher levels of purifying selection (and are consequently more conserved) because fundamental stages of embryogenesis must proceed correctly for an organism to survive (Piasecka et al. 2013). For example, Roux and Robinson-Rechavi (2008) demonstrated that genes expressed in early stages of embryogenesis are under higher constraint, and that these constraints are progressively more relaxed over the course of development. Theoretically, early stages of reiterative signaling pathways may be under similar constraint if early perturbations in the pathway result in deleterious downstream effects. In this scenario, earlier developing structures may be more developmentally canalized, and therefore less evolvable. This accords with observed patterns of developmental abnormalities in the human dentition, in which agenesis of the mandibular first molar is exceedingly rare, whereas agenesis of the M3 is

frequent enough to be considered within normal variation (Polder et al. 2004).

We can also consider variation in the M3 in terms of functional occlusal relationships and biomechanics of the jaw (Glowacka and Schwartz 2021), and how this might constrain the mutational matrix (quantified as the amount of phenotypic variance created by mutation per generation; Houle et al. 2017). For instance, if selection on the M3 is relaxed because it is less functionally constrained than the M1 and M2, it would be predicted to have a higher mutation rate and therefore be more evolvable (Bolstad et al. 2014; Jones et al. 2014) or permit higher levels of environmental variation. In the typical mammalian dentition, the upper molars occlude one half step behind the homologous lower molars (Fleagle and Kitahara-Frisch 1984). Consequently, there is no lower tooth with which the distal half of the upper M3 can occlude if all molars are approximately the same size and shape. To maintain occlusion between the distal-most molars, selection can either shorten the upper M3 or elongate the lower M3 (Fleagle and Kitahara-Frisch 1984). As a result, one might expect that adaptive peaks among species may change more rapidly for the M3 than the other molars because it is less functionally constrained, and thus its adaptive peak may take on many different values (or be wider along that axis). Therefore, relaxed selection on a particular axis of the adaptive landscape for a trait could lead to greater standing genetic variation, relaxed selection on the mutation rate, and/or higher levels of environmental variation on successive molars, because these are not as constrained and subject to less stabilizing selection.

However, how macroevolutionary divergence and selection can shape the input of mutational variation directly (Fig. 1, arrow 2) seems paradoxical given the nature of evolution, which emphasizes the current rather than the future function of traits (Wagner and Altenberg 1996; Watson and Szathmary 2016). Because developmental architecture serves as the intermediary between the genotype and phenotype, different regulatory networks can generate strong changes in the structure and alignment of mutational and environmental variance (Uller et al. 2018). These changes can potentially result in alignment of these variances and the adaptive landscape (Pavlicev et al. 2011; Hether and Hohenlohe 2013), particularly if the functional constraints reflected over ontogeny are mirrored by constraints that shape the macroevolutionary landscape (Riedl 1977; Uller et al. 2018).

Our results support the possibility that the inhibitory cascade biases divergence with "positive constraints" (Gould 1989) along macroevolutionarily divergent adaptive peaks, and that this axis of variation is aligned with the functional adaptive landscape for molar occlusion. As such, adaptation may have refined and shaped the developmental genetic architecture of the inhibitory cascade so that mutational and environmental variation is channeled along this same adaptive landscape. One prediction from such a hypothesis is that species that have experienced a history of selection gradients orthogonal to genetic variation might show evidence of changes in the regulation and/or timing of molar development that break these mechanisms promoting developmental bias, and thereby change the input of mutational and environmental variation (Navarro and Maga 2018).

Regardless of the precise mechanism, the developmental processes of molar teeth appear integral to understanding their patterns of macroevolutionary phenotypic variation (Wagner and Misof 1993; Wagner and Altenberg 1996). We argue that focusing on traits with well-understood developmental genetics can potentially elucidate the reasons for the apparent tendency for development to align with patterns of divergence between species. The results of this study lend support to the hypothesis that developmental processes have played a role in shaping the divergences of multiple anatomical regions across numerous vertebrate lineages, ranging from the avian cranium to tetrapod limbs (e.g., Sears et al. 2006; Weatherbee et al. 2006; Mallarino et al. 2011; Felice and Goswami 2017). This provides a key link for understanding how developmental processes and genetic variance impact evolutionary dynamics on a macroevolutionary scale, and enables predictions about the distribution of anatomical variation and how that variation interacts with evolutionary processes over deep time (Hlusko et al. 2016).

AUTHOR CONTRIBUTIONS

CSM conceived and designed the study with input from all authors. CSM, JCU, and FAM conducted analyses. CSM and JCU wrote the initial version of the manuscript. All authors contributed to subsequent versions of the manuscript and contributed to discussions of the proposed theoretical model.

ACKNOWLEDGMENTS

We are grateful to M. J. Plavcan for providing the dental measurement data that formed the basis of these analyses. We thank P. D. Polly, J. G. Fleagle, J. B. Rossie, and L. J. Hlusko for insights provided during helpful discussions. CSM was supported by the Gerstner Fellowship and the Gerstner Family Foundation, the Kalbfleisch Fellowship, and the Richard Gilder Graduate School of the American Museum of Natural History. Portions of this work were completed as part of a dissertation that was funded by a National Science Foundation Doctoral Dissertation Improvement Grant (National Science Foundation BCS-1613401) and a Wenner-Gren Foundation Dissertation Fieldwork Grant (Gr. 9242).

DATA ARCHIVING

All data in this study were drawn from published sources.

CONFLICT OF INTEREST

The authors declare no conflict of interest.

LITERATURE CITED

Adams, D.C. (2014) A generalized k statistic for estimating phylogenetic signal from shape and other high-dimensional multivariate data. *Systematic Biology*, 63, 685–697.

Alba, V., Carthew, J.E., Carthew, R.W. & Mani, M. (2021) Global constraints within the developmental program of the *Drosophila* wing. *eLife*, 10, e66750.

Arnold, C., Matthews, L.J. & Nunn, C.L. (2010) The 10kTrees website: a new online resource for primate phylogeny. *Evol. Anthropol.*, 19, 114–118.

Arnold, S.J. & Phillips, P.C. (1999) Hierarchical comparison of genetic variance-covariance matrices. II. Costal-inland divergence in the garter snake, *Thamnophis elegans*. *Evolution; Internation Journal of Organic Evolution*, 53, 1516–1527.

Blows, M.W. & Higgie, M. (2003) Genetic constraints on the evolution of mate recognition under natural selection. *American Naturalist*, 161, 240–253.

Bolstad, G.H., Hansen, T.F., Pélabon, C., Falahati-Anbaran, M., Pérez-Barrales, R. & Armbruster, W.S. (2014) Genetic constraints predict evolutionary divergence in Dalechampia blossoms. *Philosophical Transactions of the Royal Society B: Biological Sciences*, 369, 20130255.

Butler, P.M. (1939) Studies of the mammalian dentition—differentiation of the post-canine dentition. *Proc. Zool. Soc. Lond*, 1-36.

Cheverud, J.M. (1988) A comparison of genetic and phenotypic correlations. *Evolution; international journal of organic evolution*, 42, 958–968.

Claverie, T. & Patek, S.N. (2013) Modularity and rates of evolutionary change in a power-amplified prey capture system. *Evolution; international journal of organic evolution*, 67, 3191-3207.

Dennis, B., Ponciano, J.M., Taper, M.L. & Lele, S.R. (2019) Errors in statistical inference under model misspecification: evidence, hypothesis testing, and AIC. *Frontiers in Ecology and Evolution*, 7, 372.

Denton, J.S.S. & Adams, D.C. (2015) A new phylogenetic test for comparing multiple high-dimensional evolutionary rates suggests interplay of evolutionary rates and modularity in lanternfishes (Myctophiformes; Myctophidae). *Evolution; international journal of organic evolution*, 69, 2425-2440.

Felice, R.N. & Goswami, A. (2017) Developmental origins of mosaic evolution in the avian cranium. *Proc. Natl. Acad. Sci*, 11, 201716437-201716560.

Felsenstein, J. (1973) Maximum-likelihood estimation of evolutionary trees from continuous characters. *Am. J. Hum. Genet*, 25, 471-492.

Felsenstein, J. (1988) Phylogenies and quantitative characters. *Annu. Rev. Ecol. Syst*, 19, 445-471.

Felsenstein, J. (2008) Comparative methods with sampling error and within-species variation: contrasts revisited and revised. *The American Naturalist*, 171, 713-725.

Fleagle, J.G. & Kitahara-Frisch, J. (1984) Correlation and adaptation in the dentition of Lar Gibbons. Pp. 192–206 *in* H. Preuschoft, D. J. Chivers, W. Y. Brockelman, and N. Creel, eds. The lesser apes. Edinburgh Univ. Press, Edinburgh, U.K.

Glowacka, H. & Schwartz, G.T. (2021) A biomechanical perspective on molar emergence and primate life history. *Science Advances*, 7, eabj0335.

Gould, S.J. (1989) A developmental constraint incerion, with comments on the definition and interpretation of constraint in evolution. *Evolution; international journal of organic evolution*, 43, 516-539.

Gómez-Robles, A. & Polly, P.D. (2012) Morphological integration in the hominin dentition: evolutionary, developmental, and functional factors. *Evolution; international journal of organic evolution*, 66, 1024-1043.

Hardin, A.M. (2019) Genetic correlations in the dental dimensions of *Saguinus fuscicollis*. *Am. J. Phys. Anthropol*, 169, 557-566.

Hardin, A.M. (2020) Genetic correlations in the rhesus macaque dentition. *Journal of human evolution*, 148, 102873.

Hether, T.D. & Hohenlohe, P.A. (2013) Genetic regulatory network motifs constrain adaptation through curvature in the landscape of mutational (co)variance. *Evolution; international journal of organic evolution*, 68, 950-964.

Hlusko, L.J. (2004). Integrating the genotype and phenotype in hominid paleontology. *Proceedings of the National Academy of Sciences of the United States of America*, 101, 2653-2657.

Hlusko, L.J., Schmitt, C.A., Monson, T.A., Brasil, M.F. & Mahaney, M.C. (2016). The integration of quantitative genetics, paleontology, and neontology reveals genetic underpinnings of primate dental evolution. *Proceedings of the National Academy of Sciences*, 113(33), 9262-9267.

Hlusko, L.J. & Mahaney, M.C. (2009) Quantitative genetics, pleiotropy, and morphological integration in the dentition of papio hamadryas. *Evolutionary Biology*, 36, 5-18.

Hlusko, L.J., Sage, R.D. & Mahaney, M.C. (2011) Modularity in the mammalian dentition: mice and monkeys share a common dental genetic architecture. *The Journal of experimental zoology*, 316, 21-49.

Hohenlohe, P.A. & Arnold, S.J. (2008) MIPoD: a hypothesis-testing framework for microevolutionary inference from patterns of divergence. *The American Naturalist*, 171, 366-385.

Houle, D., Bolstad, G.H., van der Linde, K. & Hansen, T.F. (2017) Mutation predicts 40 million years of fly wing evolution. *Nature*, 548, 447-450.

Hunt, G. (2007) Evolutionary divergence in directions of high phenotypic variance in the Ostracode genus *Poseidonamicus*. *Evolution; international journal of organic evolution*, 61, 1560-1576.

Jernvall, J. & Jung, H.-S. (2000) Genotype, phenotype, and developmental biology of molar tooth characters. *Yearb. Phys. Anthropol*, 43, 171-190.

Jernvall, J. & Thesleff, I. (2000) Reiterative signaling and patterning during mammalian tooth morphogenesis. *Mechanisms of development*, 92, 19-29.

Jones, A.G., Bürger, R. & Arnold, S.J. (2014) Epistasis and natural selection shape the mutational architecture of complex traits. *Nature Communications*, 5, 3709.

Kavanagh, K.D., Evans, A.R. & Jernvall, J. (2007) Predicting evolutionary patterns of mammalian teeth from development. *Nature*, 449, 427-432.

Lynch, M. (1990) The rate of morphological evolution in mammals from the standpoint of the neutral expectation. *The American Naturalist*, 136, 727-741.

Mallarino, R., Grant, P.R., Grant, B.R., Herrel, A., Kuo, W.P. & Abzhanov, A. (2011) Two developmental modules establish 3D beak-shape variation in Darwin's finches. *Proc. Natl. Acad. Sci*, 108, 4057-4062.

McGlothlin, J.W., Kobiela, M.E., Wright, H.V., Mahler, D.L., Kolbe, J.J., Losos, J.B. & Brodie, E.D. (2018) Adaptive radiation along a deeply conserved genetic line of least resistance in Anolis lizards. *Evolution Letters*, 2, 310-322.

Melo, D., Garcia, G., Hubbe, A., Assis, A.P. & Marroig, G. (2015) EvolQG - an R package for evolutionary quantitative genetics. *F1000Research*, 4, 925-925.

Melo, D., Porto, A., Cheverud, J.M. & Marroig, G. (2016) Modularity: genes, development, and evolution. *Annu. Rev. Ecol. Syst*, 47, 463-486.

Mitov, V., Bartoszek, K. & Stadler, T. (2019) Automatic generation of evolutionary hypotheses using mixed Gaussian phylogenetic models. *Proc. Natl. Acad. Sci*, 116, 16921-16926.

Mitov, V., Bartoszek, K., Asimomitis, G. & Stadler, T. (2020) Fast likelihood calculation for multivariate Gaussian phylogenetic models with shifts. *Theor. Popul. Biol*, 131, 66-78.

Navarro, N. & Maga, A.M. (2018) Genetic mapping of molar size relations identifies inhibitory locus for third molars in mice. *Heredity*, 137, 1-11.

Pagel, M.D. & Meade, A. (2007) BayesTraits. Available via http://www.evolution.rdg.ac.ukBayesTraits.html.

Pavlicev, M., Cheverud, J.M. & Wagner, G.P. (2011) Evolution of adaptive phenotypic variation patterns by direct selection for evolvability. *Proceedings of the Royal Society B: Biological Sciences*, 278, 1903-1912.

Piasecka, B., Lichocki, P., Moretti, S., Bergmann, S. & Robinson-Rechavi, M. (2013) The hourglass and the early conservation models—co-existing patterns of developmental constraints in vertebrates. *PLoS genetics*, 9, e1003476.

Plavcan, J.M. (1990) Sexual dimorphism in the dentition of extant anthropoid primates. Ph.D. diss., Duke University, Durham, NC.

Polder, B.J., Van't Hof, M.A., Van der Linden, F.P.G.M. & Kuijpers Jagtman, A.M. (2004) A meta-analysis of the prevalence of dental agenesis of permanent teeth. *Community dentistry and oral epidemiology*, 32, 217-226.

Polly, P.D. & Mock, O.B. (2017) Heritability: the link between development and the microevolution of molar tooth form. *Hist. Biol*, 30, 53-63.

Rambaut, A., Suchard, M.A., Xie, D. & Drummond, A.J. (2014) Tracer v1.6.0. Available via http://beast.bio.ed.ac.uk/Tracer.

Revell, L.J. & Harmon, L.J. (2008) Testing quantitative genetic hypotheses about the evolutionary rate matrix for continuous characters. *Evolutionary ecology research*, 10, 311-331.

Revell, L.J. (2012) phytools: an R package for phylogenetic comparative biology (and other things). *Methods in Ecology and Evolution*, 3, 217-223.

Riedl, R. (1977) A systems-analytical approach to macro-evolutionary phenomena. *Q. Rev. Biol*, 52, 351-370.

Roff, D.A. (1995) The estimation of genetic correlations from phenotypic correlations: a test of Cheverud's conjecture. *Heredity*, 74, 481-490.

Roux, J. & Robinson-Rechavi, M. (2008) Developmental constraints on vertebrate genome evolution. *PLoS Genetics*, 4, e1000311.

Schluter, D. (1996) Adaptive radiation along genetic lines of least resistance. *Evolution; international journal of organic evolution*, 50, 1766-1774.

Sears, K.E., Behringer, R.R., Rasweiler, J.J. & Niswander, L.A. (2006) Development of bat flight: morphologic and molecular evolution of bat wing digits. *Proc. Natl. Acad. Sci*, 103, 6581-6586.

Selig, K.R., Khalid, W. & Silcox Mary, T. (2021) Mammalian molar complexity follows simple, predictable patterns. *Proc. Natl. Acad. Sci*, 118, e2008850118.

Steiper, M.E.M.E. & Seiffert, E.R. (2012) Evidence for a convergent slowdown in primate molecular rates and its implications for the timing of early primate evolution. *Proc. Natl. Acad. Sci*, 109, 6006-6011.

Uller, T., Moczek, A.P., Watson, R.A., Brakefield, P.M. & Laland, K.N. (2018) Developmental bias and evolution: a regulatory network perspective. *Genetics*, 209, 949-966.

Wagner, G.P. & Altenberg, L. (1996) Perspective: complex adaptations and the evolution of evolvability. *Evolution; international journal of organic evolution*, 50, 967-976.

Wagner, G.P. & Misof, B.Y. (1993) How can a character be developmentally constrained despite variation in developmental pathways? *Journal of evolutionary biology*, 6, 449-455.

Wagner, G.P. (1988) The influence of variation and of developmental constraints on the rate of multivariate phenotypic evolution. *Journal of evolutionary biology*, 1, 45-66.

Watson, R.A. & Szathmary, E., (2016) How can evolution learn? *Trends Ecol. Evol*, 31, 147-157

Weatherbee, S.D., Behringer, R.R., Rasweiler, J.J. & Niswander, L.A. (2006) Interdigital webbing retention in bat wings illustrates genetic changes underlying amniote limb diversification. *Proc. Natl. Acad. Sci*, 103, 15103-15107.

Young, N.M., Winslow, B., Takkellapati, S. & Kavanagh, K. (2015) Shared rules of development predict patterns of evolution in vertebrate segmentation. *Nature Communications*, 6, 6690.

Associate Editor: K. Voje
Handling Editor: M. Zelditch

Supporting Information

Additional supporting information may be found online in the Supporting Information section at the end of the article.

Table S1. Species sample sizes and means and standard errors for each molar measurement.

Table S2. Comparison between direct estimates of genetic variance in baboon molars (Hlusko et al., 2011) and maximum likelihood estimates of the evolutionary rates estimated for the tooth dimensions (BL and MD) independently. Models in bold indicate the best-fitting constrained models for each molar measurement, with neither differing significantly from the more complex free model (D statistic and p-values from a likelihood ratio test).

Figure S1. Bayesian posterior distribution of anthropoid trees constructed from aligned molecular sequence data (Arnold et al., 2010)

Figure S2. Ternary plot depicting likelihood surface for macroevolutionary model (contour plot) surrounding the estimate for the best-fitting macroevolutionary model (+) for A) Buccolingual width and B) Mesiodistal length